

# Folding Transition of the Triangular Lattice

P. Di Francesco

and

E. Gitter,

*Service de Physique Théorique de Saclay \*,  
F-91191 Gif sur Yvette Cedex, France*

We study the problem of folding of the regular triangular lattice in the presence of bending rigidity  $K$  and magnetic field  $h$  (conjugate to the local normal vectors to the triangles). A numerical study of the transfer matrix of the problem shows the existence of three first order transition lines in the  $(K, h)$  plane separating three phases: a folded phase, a phase frozen in the completely flat configuration (with all normal vectors pointing up) and its mirror image (all normal vectors pointing down). At zero magnetic field, a first order folding transition is found at a positive value  $K_c \simeq 0.11(1)$  of the bending rigidity, corresponding to a triple point in the phase diagram.

---

\* Laboratoire de la Direction des Sciences de la Matière du Commissariat à l'Energie Atomique.

## 1. Introduction

It is tempting to try to describe geometrical objects like polymers (1D) or membranes (2D) in analogy with spin systems. Natural spin variables are provided for instance by the local normal or tangent vectors to the object, while elastic properties like bending rigidity naturally translate into some nearest neighbor spin coupling. However, the correspondence between geometrical objects and spin systems can be subtle, especially in two dimensions, where geometric constraints on, say, the normals to the membrane imply local constraints on the associated spin variables. Such constraints play a crucial role for tethered membranes, *i.e.* 2D polymerized networks with fixed connectivity, since they induce a crumpling transition by stabilizing an ordered phase in a region where the unconstrained spin system would be disordered. This phenomenon was recognized in [1-5], where a continuous crumpling transition is predicted.

Such a drastic change of statistical behavior is observed in the present paper, where we consider a spin system describing the thermodynamics of folding of the regular triangular lattice, a problem first considered in [6]. Considered as a geometrical object, the lattice describes a tethered membrane skeleton, made of rigid bonds along which folds can be performed. Here we consider only *complete* foldings which result in *two-dimensional* folded configurations of the membrane. In such a process, each bond serves as a hinge between its two neighboring triangles, and is in either one of the two states: folded (with the two neighboring triangles face to face) or not (side by side)<sup>1</sup>. A folding configuration (folded state) of the system is entirely specified by the list of its folded bonds. This definition corresponds to a “phantom” membrane, where the folding process may imply self-intersections, and where one cannot distinguish in the folded state between different piling orders for superimposed triangles.

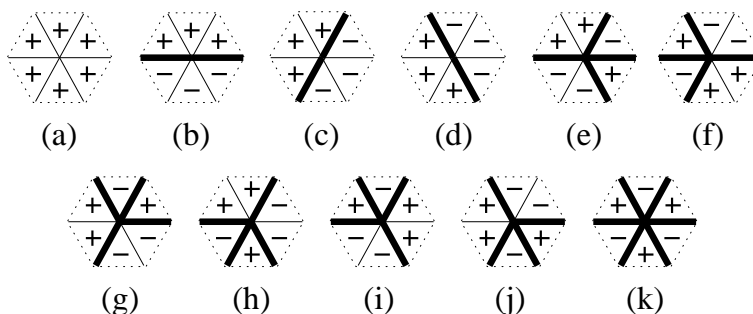


**Fig. 1:** The eleven local fold environments for a vertex. Folds are represented by thick lines. One of the two possible spin configurations on the triangles is also indicated.

<sup>1</sup> We refer the reader to [6-7] for a more formal definition of folding.

With this simplified definition, our folding problem can be formulated as an eleven vertex model, expressing that the immediate surroundings of a vertex in a folded state must be in one of the eleven local configurations depicted on Fig.1. In spite of its local definition, folding is a highly non-local operation. As explained in [7], we note that whenever a bond is folded, say, on the left half of a vertex, then another bond is folded on the right half, hence folds propagate throughout the lattice.

In a previous work [7], we have computed the exact thermodynamic entropy per triangle which counts the number  $Z_f$  of folded configurations for a finite lattice made of  $N_t$  triangles for large  $N_t \rightarrow \infty$ . This was done by mapping the eleven vertex model above onto the three-coloring problem of the triangular lattice bonds, solved exactly by Baxter [9] in its dual version, the three-coloring of the hexagonal lattice. The result reads

$$s \equiv \lim_{N_t \rightarrow \infty} \frac{1}{N_t} \text{Log } Z_f \equiv \text{Log } q$$

$$q = \prod_{p=1}^{\infty} \frac{3p-1}{\sqrt{3p(3p-2)}} = \frac{\sqrt{3}}{2\pi} \Gamma(1/3)^{3/2} = 1.20872\dots \quad (1.1)$$

As mentioned above, we will rather use here the alternative description of the model in terms of Ising spin variables  $\sigma = \pm 1$  defined on the triangles, and indicating whether they face up or down in the folded state. One can think of the spin as the normal vector to the triangle. Spin configurations are given together with the fold configurations on Fig.1. Note that there are two spin configurations for each folded state, due to the degeneracy under reversal of all spins, hence the partition function  $Z$  of the spin system is twice that of the eleven vertex model:  $Z = 2 Z_f$ . It is clear from Fig.1 that the only allowed vertex environments are those with exactly 0, 3 or 6 surrounding up spins. In order for a spin configuration to correspond to a folded state, the six spins  $\sigma_i$  around any vertex  $v$  must satisfy the *local constraint*

$$\Sigma_v \equiv \sum_{i \text{ around } v} \sigma_i = 0 \bmod 3, \quad (1.2)$$

since  $\Sigma_v = 2(\text{number of up spins}) - 6$  is a multiple of 3 iff the number of up spins itself is a multiple of 3. Beyond the above counting of the number of allowed constrained spin configurations, it would be desirable to understand the effect of a bending energy for the folds, characterizing the rigidity of the membrane. In the spin language, this means the presence of a ferromagnetic Ising-like interaction energy  $-J\sigma_i\sigma_j$  between nearest

neighbors. Most properties of the folded tethered membrane can in fact be investigated by studying the magnetic behavior of our constrained Ising spin system. The average magnetization  $M$  of the system is indeed an order parameter which is characteristic of the flatness of the membrane ( $|M| > 0$  for a configuration which is flat in average, and  $M = 0$  for a configuration which is folded in average). This suggests to introduce a magnetic field  $H$  in the system (with energy  $-H\sigma_i$  per triangle), with no direct physical meaning for the membrane, but instrumental in revealing information on its average state of folding. In the following, we will therefore consider the constrained Ising model with Hamiltonian

$$\mathcal{H}_{\text{Ising}} = -J \sum_{(ij)} \sigma_i \sigma_j - H \sum_i \sigma_i . \quad (1.3)$$

For convenience we will use the reduced coupling and magnetic field

$$K \equiv J/k_B T \quad ; \quad h \equiv H/k_B T . \quad (1.4)$$

In our study of this model, we will give numerical and theoretical evidence for the existence of a *first order transition line* in the  $(K, h)$  plane, between an ordered phase  $M = 1$  (for  $h > 0$ ) where the membrane is completely flat, and a disordered phase  $M = 0$ , where the membrane is folded and has a non-vanishing entropy. The most surprising fact is that we find no intermediary magnetization of the system in the thermodynamic limit. For  $h = 0$ , a first order folding transition still takes place, at a critical value  $K_c$  of the reduced Ising coupling  $K$ . All these results clearly show a drastic modification of the thermodynamics of the standard Ising model, emphasizing the special role played by the constraint (1.2).

The paper is organized as follows. In section 2, we describe the transfer matrix that we shall use for numerical simulations on the thermodynamics of the constrained spin system, and show how to take advantage of some particular properties of this matrix. The results for the magnetization in the presence of a magnetic field are discussed in section 3, and lead us to formulate the abovementioned two phase ( $M = 0, 1$ ) hypothesis. Under this assumption, we also derive a simple argument to calculate the critical value of the magnetic field where the transition between these phases takes place. Section 4 is dedicated to the precise study of the first order transition line in the thermodynamic limit. In particular, we find the critical value  $K_c$  beyond which the  $M = 1$  phase persists even at zero magnetic field. We discuss the general phase diagram of the system in section 5, and gather more evidence for the first order character of the transition. Related topics are discussed in section 6, including the exact solution for the square lattice as well as some predictions of a possible *antiferromagnetic transition* within the  $M = 0$  phase, for negative  $K$ . Section 7 is a brief conclusion.

## 2. Transfer matrix description

We consider the folding of an infinite strip of triangular lattice of finite width  $L$ , with free boundary conditions on the edges of the strip. Imposing periodic boundary conditions at infinity, the partition function of the model is expressed as

$$Z^{(L)}(K, h) = \lim_{N \rightarrow \infty} [\text{Tr}(T^{(L)}(K, h)^N)]^{\frac{1}{N}}, \quad (2.1)$$

where  $T^{(L)}$  denotes the transfer matrix, acting as an operator on a column of size  $L$ , whose state is specified by the  $2L$  spin values  $\sigma_i = \pm 1, i = 1, \dots, 2L$  on the triangles.

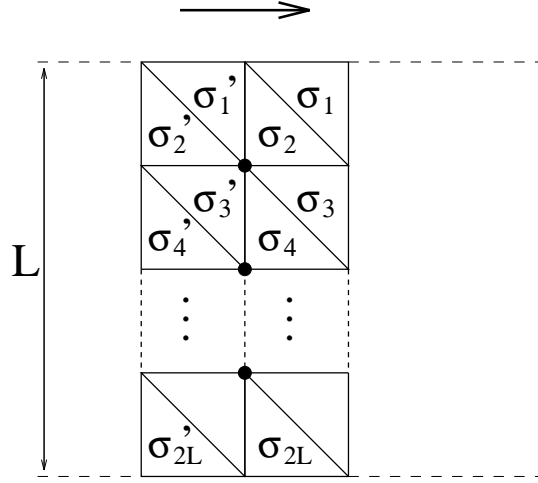


**Fig. 2:** The transfer matrix  $T^{(L)}$ .

The matrix element of  $T^{(L)}$  between two consecutive columns, as depicted on Fig.2, reads

$$T_{\{\sigma'\}, \{\sigma\}}^{(L)}(K, h) = T_{\{\sigma'\}, \{\sigma\}}^{(L)}(0, 0) U_{\{\sigma'\}, \{\sigma\}}^{(L)}(K) V_{\{\sigma'\}, \{\sigma\}}^{(L)}(h),$$

where  $T^{(L)}(0, 0)$  imposes the local folding constraint (1.2) on the six spins surrounding each of the  $L - 1$  inner vertices (marked by black dots on Fig.2), and  $U^{(L)}$  and  $V^{(L)}$  are the usual temperature and magnetic field contributions to the transfer matrix of the Ising model, namely

$$\begin{aligned} T_{\{\sigma'\}, \{\sigma\}}^{(L)}(0, 0) &= \prod_{i=1}^{L-1} \delta(\sigma_{2i} + \sigma_{2i+1} + \sigma_{2i+2} + \sigma'_{2i-1} + \sigma'_{2i} + \sigma'_{2i+1} \bmod 3) \\ U_{\{\sigma'\}, \{\sigma\}}^{(L)}(K) &= \exp\left(\frac{K}{2} \sum_{i=1}^{2L-1} (\sigma_i \sigma_{i+1} + \sigma'_i \sigma'_{i+1}) + K \sum_{i=1}^L \sigma_{2i} \sigma'_{2i-1}\right) \\ V_{\{\sigma'\}, \{\sigma\}}^{(L)}(h) &= \exp\left(\frac{h}{2} \sum_{i=1}^{2L} (\sigma_i + \sigma'_i)\right), \end{aligned}$$

with  $\delta(x)$  the usual Kronecker delta function on integers.

In the large  $N$  limit, the partition function (2.1) is dominated by the largest eigenvalue of  $T^{(L)}(K, h)$ , which we denote by  $\lambda_{\max}^{(L)}(K, h)$ , and the corresponding free energy per triangle reads

$$-F^{(L)}(K, h) = \frac{1}{2L} \text{Log } Z^{(L)}(K, h) = \frac{1}{2L} \text{Log } \lambda_{\max}^{(L)}(K, h) .$$

The thermodynamic free energy per triangle is then defined as the  $L \rightarrow \infty$  limit

$$-F(K, h) = \lim_{L \rightarrow \infty} \frac{1}{2L} \text{Log } \lambda_{\max}^{(L)}(K, h) . \quad (2.2)$$

Our main task is therefore the numerical extraction of this eigenvalue, together with the corresponding eigenvector  $v_{\max}^{(L)}(K, h)$ . We will also be interested in evaluating the subleading eigenvalue  $\lambda_{\text{sub}}^{(L)}(K, h)$ .

The analysis can be simplified in view of the following properties of the transfer matrix. Due to the local constraint on the spin variables, the matrix  $T^{(L)}(K, h)$ , of size  $2^{2L} \times 2^{2L}$ , is sparse. The exact number  $N_L$  of non-zero entries of  $T^{(L)}$  is easily computed by using the *vertical* transfer matrix of size 2,  $T^{(2)}(0, 0)$ , namely

$$N_L = \sum_{\{\sigma'\}, \{\sigma\}} \left[ T^{(2)}(0, 0)^L \right]_{\{\sigma'\}, \{\sigma\}} .$$

Diagonalizing  $T^{(2)}$  exactly, we find

$$N_L = \frac{1}{2} \left[ \left( \frac{7 + \sqrt{17}}{2} \right)^L \left\{ \frac{11 + 3\sqrt{17}}{\sqrt{17}} \right\} - \left( \frac{7 - \sqrt{17}}{2} \right)^L \left\{ \frac{11 - 3\sqrt{17}}{\sqrt{17}} \right\} \right] .$$

The first values of  $N_L$  are given in Table I below.  $N_L$  grows like  $(5.56\ldots)^L \ll 16^L$ , which justifies the use of a diagonalization algorithm adapted to sparse matrices: starting from a given vector, we compute recursively its iterated image by  $T$ , which we moreover normalize at each step; the process converges to the eigenvector  $v_{\max}$  associated to  $\lambda_{\max}$ . The subleading eigenvalue  $\lambda_{\text{sub}}$  is obtained by use of the same algorithm, together with a suitable projection procedure, guaranteeing at each step that we subtract the component along the maximum eigenvector. This projection procedure is made easy by the following symmetry property of the transfer matrix. Consider the picture of Fig.2, and rotate it by 180 degrees. One gets an identity between two transfer matrix elements, namely

$$T^{(L)}(K, h)_{\sigma'_1, \sigma'_2, \dots, \sigma'_{2L}; \sigma_1, \sigma_2, \dots, \sigma_{2L}} = T^{(L)}(K, h)_{\sigma_{2L}, \dots, \sigma_2, \sigma_1; \sigma'_{2L}, \dots, \sigma'_2, \sigma'_1}$$

This can be recast into  $T^{(L)}(K, h)^T = R T^{(L)}(K, h) R$ , where  $R$  is an involution, with matrix elements

$$R_{\sigma'_1, \sigma'_2, \dots, \sigma'_{2L}; \sigma_1, \sigma_2, \dots, \sigma_{2L}} = \prod_{i=1}^{2L} \delta(\sigma'_i - \sigma_{2L+1-i}).$$

Any eigenvector  $v$  with eigenvalue  $\lambda < \lambda_{\max}$  is then clearly orthogonal to  $R v_{\max}$ . To project out the  $v_{\max}$  component off a given vector  $w$ , one simply has to perform the substitution

$$w \rightarrow w - \frac{(R v_{\max} | w)}{(R v_{\max} | v_{\max})} v_{\max}.$$

From the knowledge of the eigenvector  $v_{\max}^{(L)}(K, h)$ , we can get the expectation value of *local* observables of the system. For instance, the magnetization  $M$  is obtained as follows. The magnetization operator  $\mu$  acts diagonally on the columns of  $2L$  spins, with diagonal elements  $\mu_{\{\sigma\}, \{\sigma\}} = \sum_{i=1}^{2L} \sigma_i$ . In the  $N \rightarrow \infty$  limit, its expectation value  $M = \langle \mu \rangle$  reads

$$M = \frac{(R v_{\max}^{(L)}(K, h) | \mu v_{\max}^{(L)}(K, h))}{(R v_{\max}^{(L)}(K, h) | v_{\max}^{(L)}(K, h))}. \quad (2.3)$$

As a test of the precision of our algorithms, we first compute  $\lambda_{\max}^{(L)}(0, 0)$  for various sizes  $L = 2, 3, \dots, 9$ . The results are summarized in Table I.

$L$	$N_L$	$\lambda_{\max}^{(L)}(0, 0)$
2	88	5.56155281
3	488	7.89397081
4	2712	11.32598261
5	15080	16.34742307
6	83864	23.67855022
7	466408	34.37351897
8	2593944	49.97256996
9	14426344	72.72483625

**Table I:** The number  $N_L$  of non-vanishing transfer matrix elements and the maximum eigenvalue  $\lambda_{\max}$  for strips of width  $L = 2, 3, \dots, 9$ .

This leads to an estimate<sup>2</sup> for the thermodynamic entropy per site  $-F(0,0) = \text{Log } q$ , with  $q = 1.208..$ , in very good agreement with a previous numerical estimate [6], and with the exact result (1.1).

### 3. Magnetization, critical magnetic field and the two phase hypothesis

As mentioned above, the magnetization  $M$  of the system is an order parameter for the flatness of the lattice. At  $K = 0, h = 0$  the system is folded in average, with a non-vanishing folding entropy  $-F(0,0)$ , therefore the magnetization  $M$  (2.3) vanishes identically. On the other hand, we will have  $M \rightarrow 1$  for sufficiently large  $h > 0$ .

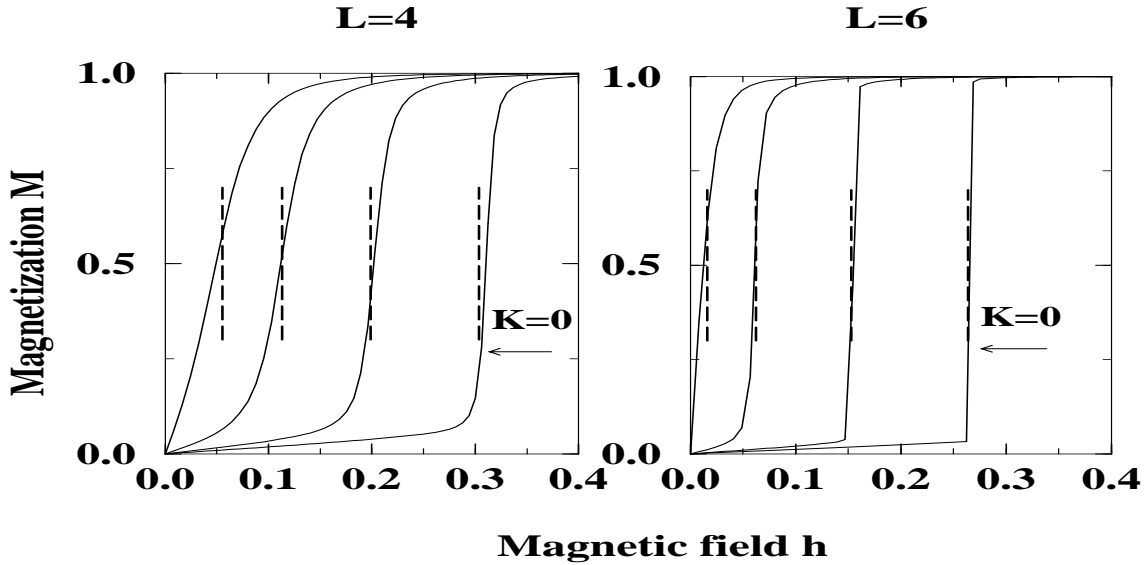


**Fig. 3:** Magnetization  $M$  versus magnetic field  $h$  for  $L = 4$  and  $6$ . The four curves correspond respectively (from the right to the left) to  $\exp(K/2) = 1$  ( $K = 0$ ), 1.0333..., 1.0666... and 1.1. The dashed vertical lines indicate the critical magnetic field  $h_c^{(L)}$  as predicted by eqn.(3.1).

Fig.3 represents the magnetization  $M$  versus the magnetic field  $h \geq 0$ , computed through the formula (2.3) for strips of width  $L = 4$  and  $6$ , for several values of  $K$ , in the range  $[0, 0.2]$ . It clearly appears, and even more so for the larger  $L$ , that the magnetization tends to remain zero over a finite range of (small enough) magnetic fields, and then abruptly jumps to 1 when  $h$  reaches some critical value  $h_c^{(L)}(K)$ . Moreover, this critical field  $h_c^{(L)}(K)$

---

<sup>2</sup> We obtain the value of  $q$  as the limit of the sequence  $q_L = \sqrt{\lambda_{\max}^{(L+1)} / \lambda_{\max}^{(L)}}$ , extracted by the Aitken delta-2 algorithm (exponential fit).



is maximal for  $K = 0$  and decreases with increasing  $K$ . For a given  $K$ ,  $h_c^{(L)}(K)$  also decreases with increasing  $L$ , eventually reaching its thermodynamic limit  $h_c(K)$  for  $L \rightarrow \infty$ .

This somewhat unexpectedly rapid change in  $M$  is the first tangible sign of the existence of a first order magnetic transition in the system. At this point, it is reasonable to infer that in the thermodynamic limit  $L \rightarrow \infty$ , and for a given coupling  $K \geq 0$ , the magnetization  $M$  is exactly zero for  $0 \leq h < h_c(K)$ , and exactly one for  $h > h_c(K)$ , being therefore discontinuous at  $h = h_c(K)$ , with  $h_c(K)$  a decreasing function of  $K$ . Indeed all our results in the following will corroborate this picture of a first order transition between two phases with respectively  $M = 0$  and  $M = 1$ , *without any possible intermediate value of the magnetization*.

A first check of the above two phase hypothesis is actually provided by the possible *derivation* of the value of the critical magnetic field through the following simple theoretical argument. Suppose that for large enough but finite strip width  $L$ , we can already describe the system in terms of two phases  $M = 0$  and  $M = 1$ . In the phase  $M = 0$  ( $h < h_c^{(L)}(K)$ ), the system is *insensitive* to the value of the magnetic field  $h$ , its partition function is therefore given by  $Z^{(L)}(K, h) \simeq Z^{(L)}(K, 0) = \exp(-2LF^{(L)}(K, 0))$ . In the flat phase  $M = 1$  ( $h > h_c^{(L)}(K)$ ), the partition function is that of the *pure state* with all spins up, hence reads  $Z^{(L)}(K, h) \simeq \exp((3L - 1)K + 2Lh)$ , since  $3L - 1$  bonds separate the  $2L$  triangles. The phase transition is then predicted to occur at the critical value of the field  $h$  where the free energies of the two phases are identical, namely

$$h_c^{(L)}(K) = -F^{(L)}(K, 0) - \frac{K}{2}\left(3 - \frac{1}{L}\right), \quad (3.1)$$

where  $-F^{(L)}(K, 0) = \frac{1}{2L} \text{Log } \lambda_{\max}^{(L)}(K, 0)$  can now be calculated numerically, directly from the *zero magnetic field* transfer matrix. The corresponding predicted values of the critical field are represented on Fig.3 by dashed vertical lines, for the various values of  $K$  and  $L$ . The agreement with the observed transition point is excellent. In the following, we shall therefore consider  $h_c^{(L)}(K)$  of eqn.(3.1) as giving the exact location of the transition point.

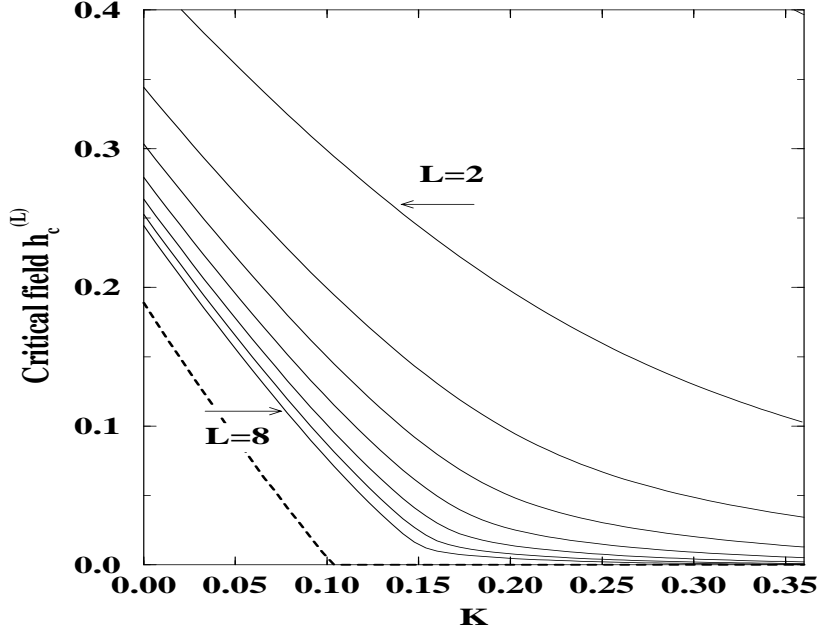


**Fig. 4:** The critical magnetic field  $h_c^{(L)}(K)$  resulting from eqn.(3.1), and the purported thermodynamic limit  $h_c(K)$  (dashed line).

#### 4. Transition line and critical coupling $K_c$

We are now interested in understanding the thermodynamic critical line  $h_c(K)$  separating, in the  $(K, h)$  phase diagram, the  $M = 0$  and  $M = 1$  phases.

On Fig.4, we have represented the curves  $h_c^{(L)}(K)$  as given by eqn.(3.1) for  $L = 2, 3, \dots, 8$  and  $K \in [0, 0.36]$ . These curves enjoy the following properties. Eqn.(3.1) expresses the critical field  $h_c^{(L)}(K)$  as the difference between the total zero field free energy and that of a particular state (the flat  $M = 1$  state):  $h_c^{(L)}(K)$  is therefore positive. It is also clear that  $h_c^{(L)}(K) \rightarrow 0$  when  $K \rightarrow \infty$  as the system gets fully ordered for strong coupling. Finally  $h_c^{(L)}(K)$  is a decreasing function of  $K$ , indeed

$$\begin{aligned} \frac{dh_c^{(L)}(K)}{dK} &= \frac{1}{2L} \sum_{(ij)} (\langle \sigma_i \sigma_j \rangle_{(K,0)} - 1) \\ &= E^{(L)}(K, 0) - \frac{1}{2} \left( 3 - \frac{1}{L} \right), \end{aligned} \quad (4.1)$$

where the sum extends over the  $3L - 1$  active bonds  $(ij)$  of a column of  $2L$  triangles, and  $E^{(L)}(K, 0)$  is the zero field average energy per triangle of a strip of width  $L$ . As  $\langle \sigma_i \sigma_j \rangle$  is always smaller or equal to one, we deduce that  $h_c^{(L)}(K)$  decreases with increasing  $K$ .

When  $L \rightarrow \infty$ , the curves  $h_c^{(L)}(K)$  of Fig.4 tend to the thermodynamic critical line  $h_c(K)$ . The properties mentioned above for finite  $L$  naturally extend to the thermodynamic limit. The critical field, now given by

$$h_c(K) = -F(K, 0) - \frac{3}{2}K, \quad (4.2)$$

is thus positive *or zero*. At  $K = 0$ ,  $h_c^{(L)}(0)$  is nothing but the entropy per triangle  $-F^{(L)}(0, 0) = \frac{1}{2L} \text{Log } \lambda_{\max}^{(L)}(0, 0)$ , with  $\lambda_{\max}^{(L)}(0, 0)$  given in Table I. Consequently, in the thermodynamic limit  $L \rightarrow \infty$ , we have the exact result

$$h_c(0) = \text{Log } q = .189\dots, \quad (4.3)$$

the transition thus taking place at a *non-zero* value of  $h$ . By continuity,  $h_c(K)$  will remain strictly positive for small positive  $K$ . Differentiating eqn.(4.2), we get

$$\begin{aligned} \frac{dh_c(K)}{dK} &= \frac{3}{2}(\langle \sigma_i \sigma_j \rangle_{(K,0)} - 1) \\ &= E(K, 0) - \frac{3}{2}, \end{aligned} \quad (4.4)$$

where  $\langle \sigma_i \sigma_j \rangle$  denotes the correlation function of *any* two neighbouring spins, and  $E(K, 0)$  is the zero field average energy per triangle of the system. Again, as  $\langle \sigma_i \sigma_j \rangle$  is always smaller or equal to one, we deduce that  $h_c(K)$  is a non-increasing function. Note that eqn.(4.4) is nothing but the Clapeyron relation

$$\frac{d}{dK} h_c(K) = -\frac{E_1 - E_0}{M_1 - M_0},$$

where  $E_i$  (resp.  $M_i$ ) denotes the Ising bending energy (resp. magnetization) in the phase  $i = 0$  or  $1$  on each side of the critical line.

Once  $h_c(K)$  is known, the  $h$  dependence of the system is determined since

$$-F(K, h) = \begin{cases} -F(K, 0) & h < h_c(K) \\ \frac{3}{2}K + h & h > h_c(K) \end{cases} \quad (4.5)$$

In turn from eqn.(4.2),  $h_c(K)$  is encoded in the zero field free energy  $-F(K, 0)$ .

A new interesting phenomenon can be read off Fig.4. For large enough  $L$ , the decrease to zero of  $h_c^{(L)}(K)$  with increasing  $K$  takes place over a finite interval  $[0, K_c^{(L)}]$ , with  $h_c^{(L)} \simeq 0$  for  $K > K_c^{(L)}$ . This is best seen on Fig.5 which represents the curves  $dh_c^{(L)}(K)/dK = E^{(L)}(K, 0) - (3L - 1)/2L$  for  $L = 2, 3, \dots, 8$  and  $K \in [0, 0.36]$ . One clearly sees a jump in the

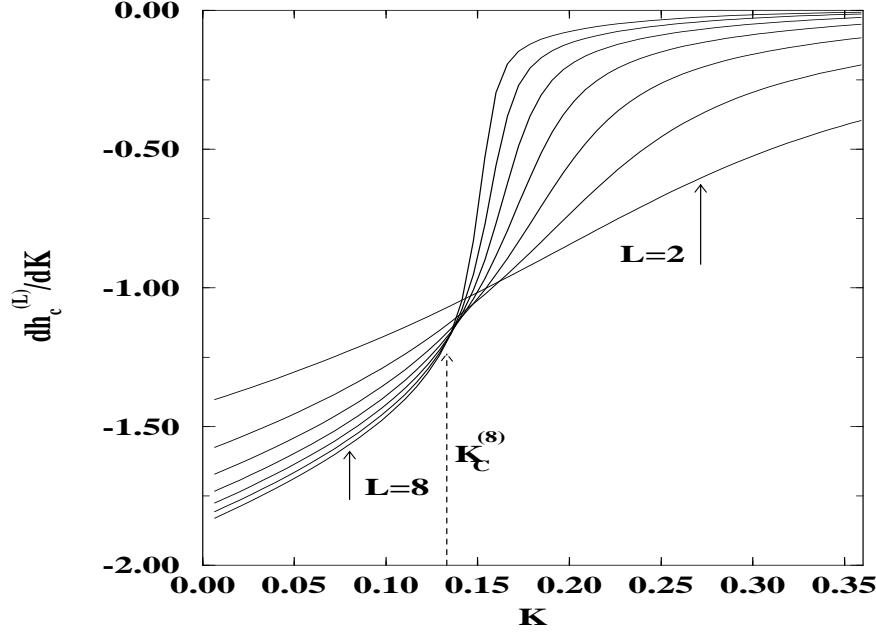


**Fig. 5:**  $dh_c^{(L)}(K)/dK = E^{(L)}(K, 0) - (3L - 1)/2L$ , for  $L = 2, 3, \dots, 8$  and  $K \in [0, 0.36]$ .

slope of  $h_c^{(L)}(K)$  from a finite value ( $\simeq -1.2$  for  $L = 8$ ) to 0. Moreover the intersections of the various curves provide us with estimates of the critical values  $K_c^{(L)}$ . The latter decrease with  $L$  and converge to a limiting value  $K_c \simeq 0.1$ .

In the thermodynamic picture, this means the existence of a critical value  $K_c$  of the coupling  $K$ , such that  $h_c(K_c) = 0$  (i.e.  $-F(K_c, 0) = \frac{3}{2}K_c$ ), and thus  $h_c(K) = 0$  for all  $K > K_c$ . On Fig.4, we have represented in dashed line the curve  $h_c(K)$  as obtained by extrapolating<sup>3</sup> to  $L = \infty$  the values of  $h_c^{(L)}(K)$  at fixed  $K$ . This direct extrapolation confirms the emergence of a critical  $K_c$  and predicts a value  $K_c = 0.11(1)$ . From Fig.5, it corresponds to  $E(K_c, 0) \simeq 0$ , *i.e.* a vanishing nearest neighbor spin correlation  $\langle \sigma_i \sigma_j \rangle \simeq 0$ .

---

<sup>3</sup> Like for our numerical estimate of  $q$ , we obtain the value  $h_c(K)$  as the logarithm of the limit of the sequence  $q_L(K) = \exp(L + 1)h_c^{(L+1)}(K)/\exp Lh_c^{(L)}(K)$ , extracted by the Aitken delta-2 algorithm.

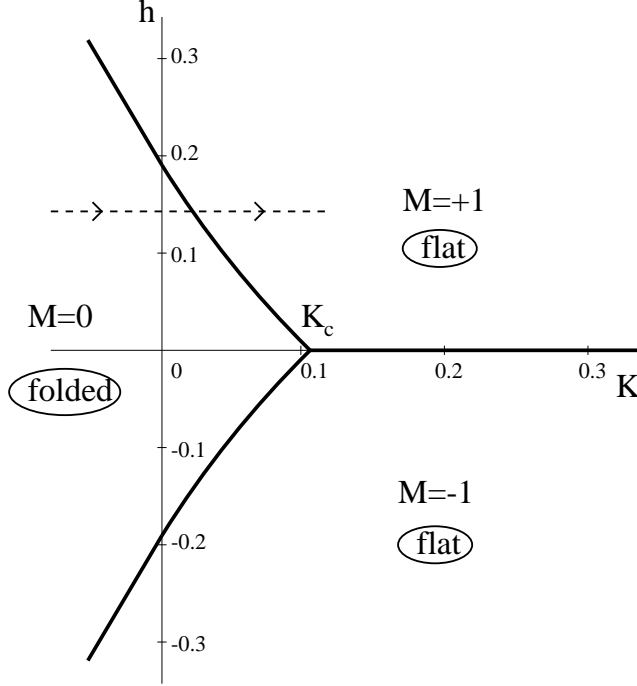


**Fig. 6:** Phase diagram in the  $(K, h)$  plane. Three first order lines  $h = h_c(K)$ ,  $-h_c(K)$  ( $K < K_c$ ) and  $h = 0$  ( $K > K_c$ ) separate the three phases  $M = 0, \pm 1$  and meet at the triple point  $(K_c, 0)$ . The dashed line represents a constant magnetic field line, which crosses the transition line  $h = h_c(K)$  at a critical value  $K_c(h)$ .

## 5. Phase diagram

Our results are summarized on Fig.6, representing the phase diagram of the system in the  $(K, h)$  plane. We extended the range of  $h$  and  $K$  to include real negative values. The phase diagram is clearly symmetric under  $h \rightarrow -h$ , while a negative  $K$  simply corresponds to an antiferromagnetic Ising coupling, which favors folding. Three first order transition lines  $h = h_c(K)$ ,  $-h_c(K)$  ( $K < K_c$ ), and  $h = 0$  ( $K > K_c$ ) separate the three phases  $M = 0, \pm 1$ . The line  $h_c(K)$  naturally extends to negative  $K$  through eqn.(3.1). For large negative  $K$ , the  $M = 0$  phase is dominated by the two pure antiferromagnetic states with alternating spins, with free energy  $-F(K, 0) \rightarrow -\frac{3}{2}K$ , hence  $h_c(K) \sim -3K$  for  $K \rightarrow -\infty$ . We expect nothing special to occur at  $K = 0$  for the line  $h_c(K)$ , where we have the exact result  $h_c(0) = \text{Log } q = .189\dots$ . Instead our study predicts the existence of a triple point  $(K_c, 0)$  at the *positive* value  $K_c \simeq .11(1)$ . For the physical zero magnetic field membrane problem, this corresponds to a *first order folding transition* at  $K = K_c$ . Within the domain  $M = 0$ , the system is insensitive to the magnetic field  $h$ . Along the constant magnetic field dashed line of Fig.6, with  $K$  increasing from  $-\infty$ , the free energy of the system is

$-F(K, 0)$  until one reaches the critical line  $K = K_c(h)$  (inverse of  $h = h_c(K)$ ), beyond which the free energy becomes the linear function  $-F(K, h) = \frac{3}{2}K + h$ .

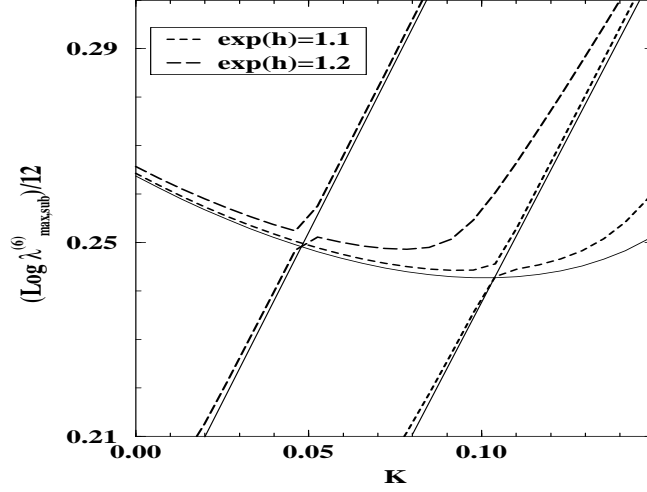


**Fig. 7:** Plot in dashed lines of  $\frac{1}{2L}\text{Log } \lambda_{\max, \text{sub}}^{(L)}(K, h)$  for  $L = 6$ ,  $\exp(h) = 1.1$  (short dashes) and  $\exp(h) = 1.2$  (long dashes), and  $K \in [0, 0.15]$ . The solid lines represent the free energies  $-F_1^{(6)}(K, h) = h + 17K/12$ , and  $-F_0^{(6)}(K, 0)$ . The crossings occur at the critical couplings  $K_c^{(6)}(\text{Log } 1.2) \simeq 0.05$  and  $K_c^{(6)}(\text{Log } 1.1) \simeq 0.10$ .

As usual for first order transitions in the transfer matrix formalism, this change of behavior results from the crossing of the two largest eigenvalues  $\lambda_{\max}$  and  $\lambda_{\text{sub}}$  of the transfer matrix  $T$  in the thermodynamic limit. Indeed this is already visible for finite  $L$ , as exemplified on Fig.7, where we plot for  $L = 6$  (in dashed lines) the two leading eigenvalues of  $T^{(6)}(K, h)$  for two different positive values of  $h$ , in the vicinity of the corresponding critical points  $K_c^{(6)}(h)$ . One clearly sees the exchange of the two eigenvalues with

$$\frac{1}{2L}\text{Log} \begin{Bmatrix} \lambda_{\max} \\ \lambda_{\text{sub}} \end{Bmatrix} = \begin{cases} \begin{Bmatrix} -F_0^{(L)} \\ -F_1^{(L)} \end{Bmatrix} & K < K_c^{(L)}(h) \\ \begin{Bmatrix} -F_1^{(L)} \\ -F_0^{(L)} \end{Bmatrix} & K > K_c^{(L)}(h) \end{cases},$$

where  $-F_1^{(L)}(K, h) = h + (3L - 1)K/2L$ , and  $-F_0^{(L)}(K, h) = -F^{(L)}(K, 0)$  denote respectively the free energy in the phase with magnetization  $M = 1$  and 0, represented for  $L = 6$  on Fig.7 in solid lines.

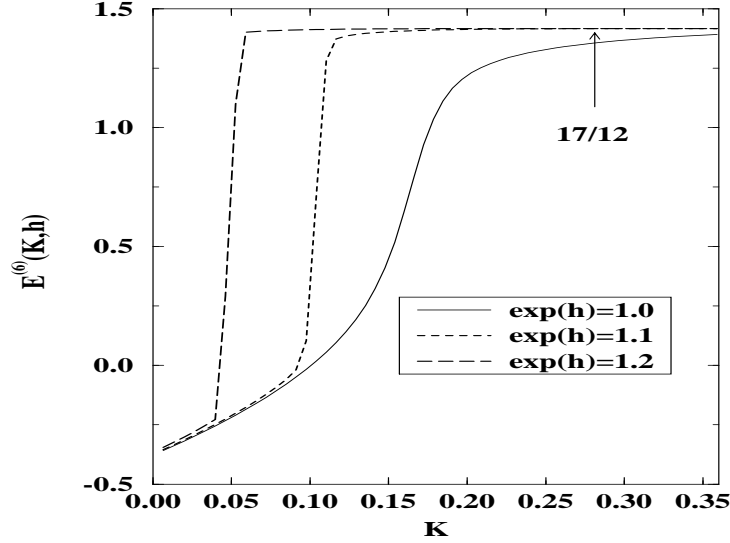


**Fig. 8:** Finite (dashed) and zero (solid) field energy versus Ising coupling, for  $L = 6$  and  $\exp(h) = 1.2, 1.1, 1$  respectively, and  $K \in [0, 0.36]$ .

The change of behavior of the free energy along a constant-field line at  $K_c(h)$  is confirmed at finite  $L$  by the plot of its derivative w.r.t.  $K$ , the Ising energy  $E^{(L)}(K, h) = -\partial_K F^{(L)}(K, h)$ , which we represent on Fig.8 for  $\exp(h) = 1, 1.1, 1.2$  and  $L = 6$ . We clearly see that the finite field energies  $E^{(6)}(K, h)$  exactly match the zero field energy  $E^{(6)}(K, 0)$  before  $K$  reaches the critical value  $K_c^{(6)}(h)$ , where they abruptly jump (the more so for higher  $h$ ) to the asymptotic value  $(3 \times 6 - 1)/(2 \times 6) = 17/12$ .

The corresponding specific heat  $C_v^{(L)}(K, h) = \partial_K E^{(L)}(K, h)$  is represented on Fig.9 for  $L = 6$  in dashed ( $\exp(h) = 1.1, 1.2$ ) and thick solid ( $\exp(h) = 1$ ) lines. As expected, the finite field specific heats match the zero field specific heat until  $K$  reaches  $K_c^{(6)}(h)$ , where they exhibit a delta-function peak, before immediately (the more so for higher  $h$ ) reaching a zero value. The peak for  $h = 0$  seems to be qualitatively different from that for finite  $h$ . To see how this peak develops as the size  $L$  grows, we have represented on the same figure the zero field specific heat for  $L = 2, 3, \dots, 8$  in thin solid lines. The smoothness of

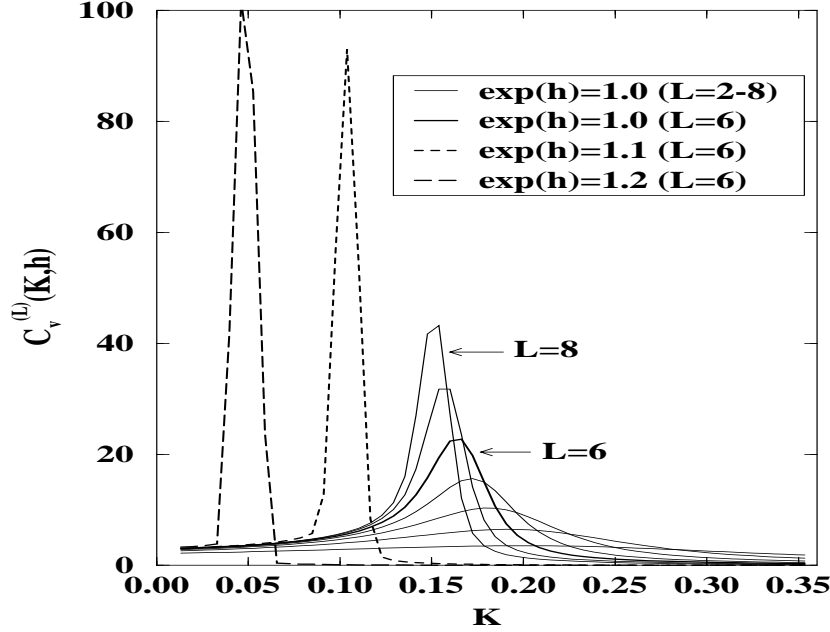


**Fig. 9:** Specific heat  $C_v^{(6)}(K, h)$  for  $\exp(h) = 1$  (thick solid line), 1.1 and 1.2 (dashed lines) and  $C_v^{(L)}(K, 0)$  for  $L = 2, 3, \dots, 8$ , for  $K \in [0, 0.36]$ .

the curves might be the sign of some extra divergence on top of the delta-function in the thermodynamic specific heat  $C_v(K, 0)$ , possibly of the form  $C_v(K, 0) \sim (K_c - K)^{-\alpha}$  when  $K$  approaches the triple point from below. Our data do not allow us at present to reach any conclusion on this point.

## 6. Discussion

The main result of this paper is the phase diagram of Fig.6. In particular, the existence of a triple point ( $K = K_c > 0, h = 0$ ) at the boundary of the three phases with magnetization  $M = 0, \pm 1$  is a non-trivial outcome of our study. It is interesting to note that a very similar picture can be obtained *exactly*<sup>4</sup> in the case of the folding of the *square* lattice. As already noted in [6], the thermodynamic entropy of folding  $-F_{\text{square}}(0, 0)$  of

---

<sup>4</sup> An exact solution can be obtained for instance by using a transfer matrix which is diagonal in terms of folded line variables.



the square lattice *vanishes*, due to the very strong constraint that, for this particular lattice, folds must propagate along straight lines, all the way through the lattice. A folded state of the square lattice is entirely specified by the data of its folded horizontal and vertical lines. For a square lattice of size  $L \times L$ , this leads to a free energy per square  $-F_{\text{square}}(0,0) = \lim_{L \rightarrow \infty} \frac{1}{L^2} \text{Log } 4^L = 0$ , as annouced. Like in the triangular case, the square lattice folding problem is easily transformed into a (face) square lattice Ising spin system, with the local constraint that there are exactly 0, 2 or 4 spins up around each vertex. The zero field thermodynamic free energy  $-F_{\text{square}}(K,0)$  per square at an arbitrary value of the reduced Ising coupling  $K$  is easily obtained as follows: at  $K = 0$ , it vanishes; for  $K \rightarrow \infty$ , it tends to the flat state value  $2K$ ; for  $K \rightarrow -\infty$ , it tends to the completely folded state value  $-2K$ . From the usual convexity property of  $-F$ , we conclude that necessarily

$$-F_{\text{square}}(K,0) = 2|K| .$$

The free energy appears here simply as a competition between the contribution of the completely folded state  $-F_0(K,0) = -2K$  and that of the flat state  $-F_1(K,0) = 2K$ , with  $-F_{\text{square}}(K,0) = \text{Max}(-F_0, -F_1)$ . Analogously, in the presence of a finite positive magnetic field  $h$ , the free energy results from the competition between the contribution of the completely folded state, insensitive to  $h$ ,  $-F_0(K,h) = -2K$ , and that of the flat (all spins up) state  $-F_1(K,h) = 2K + h$ . This yields

$$-F_{\text{square}}(K,h) = \text{Max}(-F_0(K,h), -F_1(K,h)) = \begin{cases} -2K & K < -h/4 \\ 2K + h & K > -h/4 \end{cases} .$$

Consequently the system undergoes a first order phase transition from the completely folded state with magnetization  $M = 0$  to the flat state with  $M = 1$ , along the critical line

$$h_{c,\text{square}}(K) = 2(|K| - K) ,$$

the square lattice analogue of eqn.(3.1).

As shown on the resulting phase diagram of Fig.10, the qualitative behavior of the system is very similar to the triangular case discussed above, corroborating a posteriori the diagram of Fig.6. A crucial difference is that the triple point now sits at the origin of the  $(K,h)$  plane, i.e.  $K_{c,\text{square}} = 0$ . Consequently no folding transition occurs at positive  $K$  for the square lattice, which remains flat. That  $K_c$  is positive for the triangular lattice follows directly from the positivity of the entropy at  $K = 0$ , which makes the triangular case more interesting.

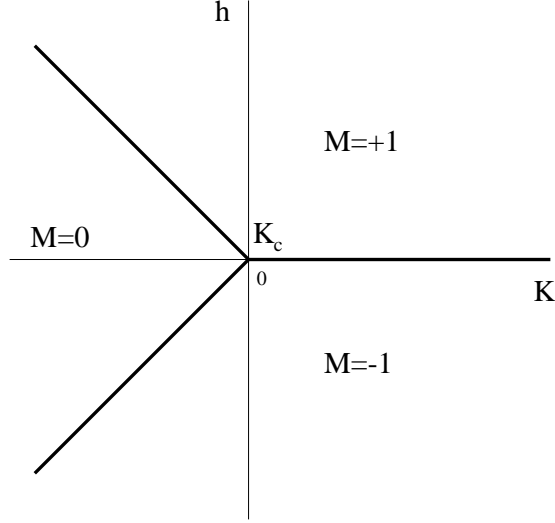


**Fig. 10:** Phase diagram of the square lattice folding problem.

A surprising outcome of our study of the triangular lattice case is the absence of intermediate magnetization states between  $M = 0$  and  $M = 1$ . Denoting by  $-F_m(K, 0)$  the contribution of the configurations with magnetization  $M = m$  to the zero field free energy, a sufficient condition for having no intermediate magnetization is that the critical field  $h_{c,m}(K)$  governing the transition between the  $M = 0$  and an hypothetical  $M = m$  phase be always larger than  $h_{c,1}(K) = h_c(K)$ , for  $K < K_c$ , namely

$$h_{c,m}(K) = \frac{-F(K, 0) + F_m(K, 0)}{m} > h_{c,1}(K) = -F(K, 0) + \frac{3}{2}K ,$$

with  $m < 1$ . The freezing of the system for  $K > K_c$  in, say, the  $M = 1$  phase is probably a consequence of the intrinsically non-local character of the folding constraint, preventing the creation of bounded domains of down spins inside a groundstate of up spins.

The stability of the  $M = 0$  phase at positive  $K$  in the presence of a magnetic field  $h < h_c(K)$  is more surprising. A way of refining the study of the  $M = 0$  phase is to introduce a new order parameter, the staggered magnetization

$$M_{\text{st}} = \frac{1}{N_t} \langle \left( \sum_{\triangle} \sigma_i - \sum_{\nabla} \sigma_i \right) \rangle ,$$

where the sum alternates between triangles pointing up and down in the lattice. One can then distinguish between the disordered folded state  $M_{\text{st}} = 0$  and a compactly ordered folded state  $M_{\text{st}} > 0$  where the triangles start to pile up. In the presence of a staggered magnetic field, we expect the system to behave qualitatively like an antiferromagnetic

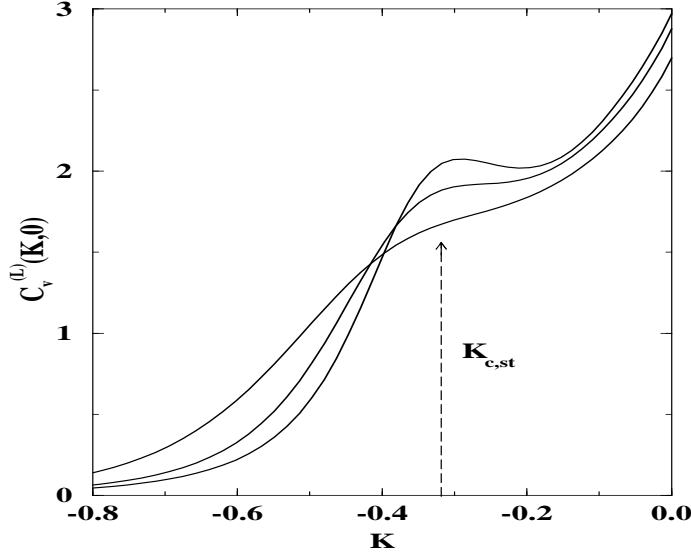


**Fig. 11:** Heat capacity  $C_v^{(L)}(K, 0)$  for  $L = 4, 6, 8$  and  $K \in [-0.8, 0]$ .

(face) triangular Ising model, with a continuous “piling” transition at some negative value of the coupling  $K_{c,st} < 0$ .

Indeed, as explained in [7], the situation is very different when we start to *unfold* the antiferromagnetic  $M_{st} = 1$  groundstate than when we try to *fold* the ferromagnetic  $M = 1$  one. Local deformations of the completely folded groundstate are allowed and enable a “low temperature” (large negative  $K$ ) expansion in terms of a gas of loops of unfolded bonds, quite similar to the standard loop gas expansion of the Ising model. As far as numerical results are concerned, we only see on Fig.11 the slow emergence of a peak in the specific heat at a value  $K_{c,st} \simeq -0.3$ . At  $K = 0$ , an exact solution [9] predicts a disordered folded state  $M_{st} = 0$  with finite staggered susceptibility.

## 7. Conclusion

In this paper, we have derived the phase diagram of the constrained spin system describing the folding of the triangular lattice. In the presence of a magnetic field, we found a critical line along which a first order transition takes place between a zero magnetization phase and the  $M = 1$  pure state, terminating at a triple point ( $K = K_c, h = 0$ ). This

transition persists at zero magnetic field, now driven by the coupling  $K$ , and can be interpreted as a *first order folding transition* between a folded phase and the completely flat state of the lattice. The latter is reminiscent of the crumpling transition of tethered membranes [1-4], which is however continuous rather than first order.

The phase diagrams of Fig.6 and 10 are very far from the usual unconstrained Ising ones. It would be interesting to investigate the role of the local folding constraint by applying it gradually to the Ising model, and by looking at the deformation of the phase diagram. In this framework, one should be able to follow the evolution of the system from a continuous second order phase transition to a first order one. Note that in the square case both the Ising and constrained models are special cases of the eight vertex model in an electric field, yet to be solved.

## Acknowledgements

We are grateful to A. Billoire, R. Lacaze and V. Pasquier for useful discussions, and especially to O. Golinelli for sharing with us his experience in numerical calculations. We thank Th. Jolicœur for a careful reading of the manuscript.

## References

- [1] D.R. Nelson and L. Peliti, J. Phys. France **48** (1987) 1085.
- [2] Y. Kantor and D.R. Nelson, Phys. Rev. Lett. **58** (1987) 2774 and Phys. Rev. **A 36** (1987) 4020.
- [3] M. Paczuski, M. Kardar and D.R. Nelson, Phys. Rev. Lett. **60** (1988) 2638.
- [4] F. David and E. Gitter, Europhys. Lett. **5** (1988) 709.
- [5] see also M. Baig, D. Espriu and J. Wheeler, Nucl. Phys. **B314** (1989) 587; R. Renken and J. Kogut, Nucl. Phys. **B342** (1990) 753; R. Harnish and J. Wheeler, Nucl. Phys. **B350** (1991) 861.
- [6] Y. Kantor and M.V. Jarić, Europhys. Lett. **11** (1990) 157.
- [7] P. Di Francesco and E. Gitter, Europhys. Lett. **26** (1994) 455.
- [8] R.J. Baxter and S.K. Tsang, J. Phys. **A13** Math. Gen. (1980) 1023.
- [9] R.J. Baxter, J. Math. Phys. **11** (1970) 784 and J. Phys. **A19** Math. Gen. (1986) 2821.